

# Atomistic measurement of the effect of interface tuning on the toughening and failure mechanisms of polypropylene nanocomposites toughened with nanofibrillated rubber

Mahdi Zeidi<sup>1\*</sup>, Chun Il Kim<sup>2</sup>, Chul B. Park<sup>1</sup>

<sup>1</sup>Department of Mechanical and Industrial Engineering, University of Toronto, Toronto, ON, Canada

<sup>2</sup>Department of Mechanical Engineering, University of Alberta, Edmonton, AB, Canada

\*[m.zeidi@mail.utoronto.ca](mailto:m.zeidi@mail.utoronto.ca)

**Abstract**—In the present study, we investigate the roles of interface and interfiber interactions on the toughening and failure mechanisms of nanofibrillated rubber-toughened thermoplastic-based nanocomposites. Emphasis is placed on establishing a comprehensive theoretical and atomistic descriptions of the nanocomposite systems subjected to pull-out and uniaxial tests. Using the framework of molecular dynamics, the annealed melt-drawn nanofibers were spontaneously formed via the proposed four-step methodology. The generated nanofibers were then crosslinked using the proposed robust topology-matching algorithm, through which the chemical reactions arising in the crosslinking were closely assimilated. The interfiber interactions were also examined with respect to separation distances and nanofiber radius via nanofiber pair atomistic scheme and the obtained results were subsequently incorporated into the pull-out and uniaxial tests simulations. The results indicate that the compatibilizer grafting results in enhanced interfacial shear strength by introducing extra chemical interactions at the interface. In particular, it was found that the compatibilizer restricts the formation and coalescence of nanovoids, resulting in enhanced toughening effects. Together, we have shown that the presence of a small amount of well-dispersed rubber nanofibrillar network whose surfaces are grafted with maleic anhydride compatibilizer can dramatically increase the toughness and alter the failure mechanisms of the nanocomposites without deteriorating stiffness which is also consistent with the recent experimental observations. The interfacial failure mechanism was also investigated by monitoring of the changes in the atomic concentration profiles, mean square displacement and fractional free volume.

*molecular dynamics; toughening; nanofibrillated rubber; interface; crosslinking; coalescence*

## I. INTRODUCTION

There has been a growing interest in nanofibrillated polymer nanocomposites (PNCs) owing to the tunability of the properties and the capability of developing a new generation of multifunctional nanostructured materials. Unlike traditional composites, PNCs offer great opportunities to design advanced

material systems with extraordinary properties which are highly dependent on the characteristics of nanofillers and, more importantly, their interface with matrix. PNCs also exhibit a weight advantage over traditional composites because well-dispersed nanofillers with small amount can have better reinforcement effect than 20-30 wt.% microfillers. However, toughening mechanisms of nanofillers, without deteriorating overall stiffness of PNCs, have not been well understood due to the fact that stiffness and toughness are two mutually exclusive properties. The enhanced properties can be explained by two major mechanisms at the nanoscale: interface effects and inter-nanofiller interactions. Due to the greater interfacial area per unit volume of the nanofillers compared to the micro-sized fillers, the inter and intramolecular interactions at interface are intensified which facilitate load transfer from matrix to nanofiller. Besides the interface, inter-nanofiller distances approach atomic dimensions even with small amount of nanofillers which would result in having morphological-controlled properties in PNCs. Thus, the grasping of the defining roles of interface and interfiller interactions on macroscale properties is the main key in the design and accurate predictive modeling of PNCs. The interface with distinct physico-chemical and frictional characteristics determines the efficiency of load transfer from matrix to nanofiller. Therefore, characteristics of the interface may be tuned in a way to improve the interfacial load transfer and also, in some cases, to enable the interface with functional properties. Although in a few continuum-based models [1-3], researchers had taken into account the effect of waviness and aspect ratio, they underrated the effect of interface and discrete nature of the polymer materials at the nanoscale so that their models may not be applicable for nanomaterials.

The main toughening mechanisms observed in rubber nanofiber-reinforced nanocomposite are crazing and localized bands of intense shear deformation induced by stress whitening, nanovoid development and shear banding. These mechanisms have been extensively studied in the literature, including the development of theoretical and analytical prediction models for the analysis and characterization of rubber nanofiber reinforced PNCs, which are also in a period of active study [4]. For instance, in the past decades, a few advances in the modeling of toughening mechanisms have been made, and some new theories have been proposed, such as shear-yielding theory, multiple-

crazing theory and shear band/crazing interaction theory. However, predictions from theoretical models are often quite deviated from the experimental results, for example, the estimated toughness and yield strength from the theoretical models are usually far greater than those measured on fabricated nanocomposite samples. This discrepancy is mainly due to the weak interfacial adhesion and the possible nonuniformity of morphological structures at the interface, which hinder the load transfer from matrix to nanofibers during the deformation and, therefore, the objective of efficient rubber toughening cannot be fully achieved in actual field applications. Despite the extensive volume of literature that has been devoted to the study of rubber toughening mechanisms and the structure-property-processing relationships in PNCs, the understanding of toughening mechanisms and ultimate strength improvement by the introduction of rubber nanofillers still remains in its infancy, due to the complex nature of polymer nonstructural features and lack of reliable experimental data at the nanoscale. As a result, the development of such hierarchical nanomaterials is still heavily reliant on empirical approaches, so that the uses of prediction models describing the mechanics of PNCs are substantially limited.

Accurate representation of the interfiber interactions is one of the other challenges in the modeling of three-dimensional entangled fibrous networks (FNs) in PNCs, due to lack of experimental measurement techniques of interfiber interactions at the nanoscale. Various research groups tried to address this by integrating the interaction effects into their microscale models of FNs. Despite the efforts on modeling of interfiber interactions, to the best of authors knowledge, there has been no additional endeavors in verifying the results by employing nanoscale experimental techniques. Experimental measurements of interfiber interactions can be considered as the most direct method. Nevertheless, practical challenges exist such as difficulties in nanofiber sample preparations and uncertainties in recording force and energy at nanoscale, which make the experiments very costly and challenging. To overcome these issues, various finer-scale simulation techniques such as MD and quantum mechanics (QM) can be used in replacement of experiments. For instance, Buell et al. [5] employed MD simulation for analysis of interfiber interactions among polymeric nanofibers, in order to develop interfiber interaction model. Although, in their analysis, an interfiber potential energy model was proposed, the potential has not been further implemented into the large-scale MD simulation of PNCs to investigate the crucial effect of interfiber interactions on the overall fundamental properties. Therefore, the development of such a comprehensive “atomistic model” that would incorporate interaction among polymeric nanofibers into force field is greatly desired.

In order to investigate the aforementioned roles of interface and interfiber interactions, we consider the case of ethylene-propylene-diene-rubber (EPDM) nanofiber-reinforced polypropylene (PP) nanocomposites. PP is a highly versatile thermoplastic and is considered as one of the most promising materials which replace metallic components of engineering structures used in long-life applications for their high melting temperature, good processibility and mechanical performance, low cost and reduced chemical inertness. At the same time, PP

poses some noticeable disadvantages such as poor ductility and low fracture strain due to the presence of distinct spherulite boundaries. The ductility and strength of PP can, however, be enhanced by adding nanofillers as reinforcing additives. Among the nanofillers, experiments have manifested that well-dispersed elastomeric nanofillers such as EPDM are one of the most effective additives such that even a very small amount can simultaneously improve the stiffness and toughness of PP.

## II. METHODS AND SIMULATION PREPARATION

### A. Interatomic Potentials

The effects of interface on the mechanical properties of the nanocomposite systems were examined with and without the presence of maleic anhydride (MA) compatibilizer agent. The atomic systems of the nanofiber and matrix were described using a modified version of the optimized potentials for liquid simulations (OPLS) force field. The non-bonded interactions were modeled with using the 12-6 Lennard-Jones (LJ) potential.

#### 1) Bond Dissociation: Failure

Nonlinear hyperelastic behavior and failure in polymer materials are mainly due to the initiation of inter and intramolecular bond dissociation. Thus, bond dissociation and topology changes must be allowed in models to successfully simulate the failure processes. In this study, the non-reactive OPLS-UA force field was modified to accommodate the bond dissociation. In the conventional non-reactive force field, the bond dissociation is not originally incorporated in the potential functions since the chemical bonds are represented by harmonic functions. This further prevents non-reactive simulations to be employed for the failure analysis. In addition, although the reactive force fields are the best option for simulation of the chemical reactions, their computational cost are much higher than for non-reactive force fields. To overcome these issues, the bond stretching, and angle potential functions are modeled by the Morse-type and anharmonic potentials. The parameters in the Morse-type potential can be obtained by a series of QM simulations. The functional forms of the dissociative potential energies for bond length,  $E_{\text{bond}}^{\text{Dissociative}}(r, \theta)$  and angle,  $E_{\text{angles}}^{\text{Dissociative}}(\theta)$  are described by:

$$\begin{aligned} E_{\text{bond}}^{\text{Dissociative}}(r, \theta) &= [D - E_{\text{angles}}^{\text{Dissociative}}(\theta)] [1 \\ &\quad - \exp(-\alpha(r - r_0) - \beta(r - r_0)^2)]^2, \\ E_{\text{angles}}^{\text{Dissociative}}(\theta) &= k_1(\theta - \theta_0) + k_2(\theta - \theta_0)^2 + k_3(\theta - \theta_0)^3 \\ &\quad + k_4(\theta - \theta_0)^4, \end{aligned} \quad (1)$$

where  $D$  is the dissociation energy of chemical bonds when bending angle,  $\theta$ , is in equilibrium,  $\alpha$  and  $\beta$  are the fitting parameters obtained from the QM calculations, and  $k_1$  to  $k_4$  are anharmonic constants. By integrating Eq. (1), the modified OPLS-UA potential energy of the  $k^{\text{th}}$  bond length and the  $l^{\text{th}}$  bond angle can be expressed as:

$$\begin{aligned} E_{\text{total}}^{\text{Dissociative}} &= E_{\text{bond}}^{\text{Dissociative}}(r_k, \theta_l) + E_{\text{angles}}^{\text{Dissociative}}(\theta_l) + \sum_{i \neq k}^{N_b} E_{\text{bond}}(r_i) \\ &\quad + \sum_{i=1}^{N_a} E_{\text{angle}}(\theta_i) + \sum_{i=1}^{N_d} E_{\text{dihedrals}}(\Phi_i) \\ &\quad + \sum_{i=1}^{N_1-4} \sum_{l > j} E_{\text{non-bonded}}(\bar{r}_{ij}) \end{aligned} \quad (2)$$

From the QM calculations, the bond and angle force field parameters were obtained by changing the atom separation distance and angle by a magnitude of 0.05 Å and 5°.

### 2) Interface: Bonded and Non-bonded Interactions

In the case of atomistic structure of the nanocomposite system with the presence of compatibilizer agents, MA groups were added at the interface and modeled as modified OPLS-UA. The chemical structures of the PP-graft-maleic anhydride (PP-g-MA), EPDM-graft-maleic anhydride (EPDM-g-MA) and schematic illustration of MA groups at the interface are depicted in Figs. 1a-c. As shown in Fig. 1c, the two ends of the MA compatibilizer; MA-end-1 and MA-end-2, are connected to a PP matrix atom (pm1) and EPDM nanofiber atom (nf1), respectively. The total force acting on the atom nf1 in the nanofiber was then measured by the summation of (a) the calculated force of atom nf1 for the system without the presence of compatibilizer, and (b) the calculated force of MA-end-2 considering only the compatibilizer group. The total force acting on the atom pm1 was similarly measured by the same procedure. The positions of the atoms nf1 and pm1 were subsequently updated by solving the Newtonian equations of motion. In the present simulations, atom MA-end-1 is always connected with atom pm1, while the connection of the other end, MA-end-2, is determined based on the minimum energy criteria. During the simulation, there are two possible scenarios for the compatibilizer atom MA-end-2, either (a) completely detached from the EPDM, or (b) transferred from the reference position to another adjacent “possible” position. This transferring mechanism was implemented based on minimum energy criteria.

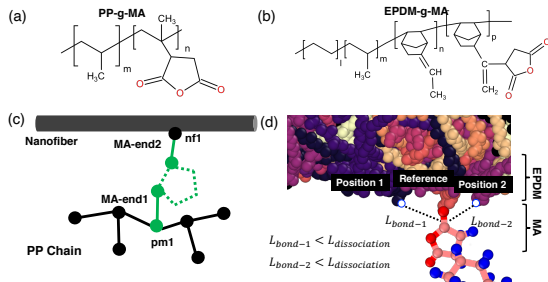


Figure 1. (a) PP-graft-maleic anhydride (PP-g-MA) chemical structure, (b) EPDM-graft-maleic anhydride (EPDM-g-MA) chemical structure, (c) schematic of the EPDM nanofiber with a PP polymer chain and a MA compatibilizer chain, and (d) switching mechanism at the interface

### B. Formation of the Nanofiber Atomistic Structure

The generation of a single free-standing annealed melt-drawn EPDM nanofiber is done using a proposed four-step methodology. The summary of this methodology is schematically depicted in Fig. 2.

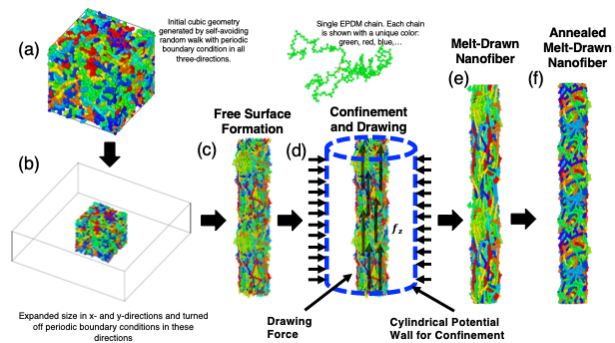


Figure 2. Spontaneously formation of nanofibers: (a) initial cubic structure generated by the self-avoiding random walk method with periodic boundary conditions, (b) expanded size in x and y-directions with turned off periodic boundary conditions, (c) spontaneously-formed nanofiber (d) applying a linear force and adding a cylindrical wall confinement to preserve the shape of the nanofiber, (e) melt-drawn nanofiber, and (f) final structure.

A schematic illustration of the effect of the melt-drawing and annealing process on the chain orientation and bonds length in the EPDM nanofiber is depicted in Fig. 3. During the melt-drawing process, due to the applied force on the molten state, the polymeric chains tend to realign along the nanofiber axis, and bond lengths are extended out of their equilibrium length and are then locked on nanofiber solidification. The interplay of these mechanisms (chain re-orientation and bond length extension) is the main reason for the simultaneous increases in the stiffness and strength of nanofibers.

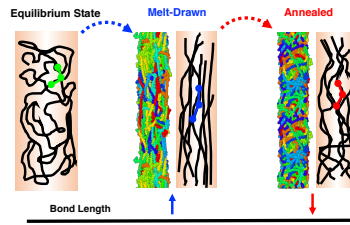


Figure 3. Schematic of the processing effects on the chain reorientation and bonds length extension of the nanofiber.

## III. MODEL IMPLEMENTATION AND METHODOLOGY

### A. Photo-Crosslinking of EPDM

The crosslinking of the EPDM is of central importance to achieve the objective of toughening in EPDM-toughened polymer blends. The crosslinking can enhance the melt tenacity, toughness and strength of the nanofiber phase which will result in fine and more consistent dispersion in the matrix. In addition, crosslinking helps the EPDM nanofibers to preserve their geometry/shape during processing at elevated temperature above the melting point. In the case of the EPDM/PP blend, the crosslinked EPDM phase act as nucleating agents and, hence, reduces the size of the small, crystalline PP spherulites that form in the PP, which may modify the mechanical performance of the resulting blend, especially fracture toughness. It was also demonstrated that crosslinking the EPDM gives rise to enhanced impact resistance of the blend without compromising stiffness, strength and processability. The aim here is to simulate the ultraviolet photo-crosslinking reaction mechanism

of the EPDM by employing the MD method. The crosslinking simulation was performed on the nanofibers by predefinition of the pre-reaction topology (before the crosslinking), post-reaction (after the crosslinking) topology, reaction map file and reaction cut-off distances. The definition of the post-reaction topology was done based on experimental studies of the photocrosslinking of EPDM. After defining the pre-reaction and post-reaction topologies, the superimpose algorithm was implemented to identify the eligible reaction sites in the simulation box. The summary of the crosslinking algorithm is shown in Fig. 4.

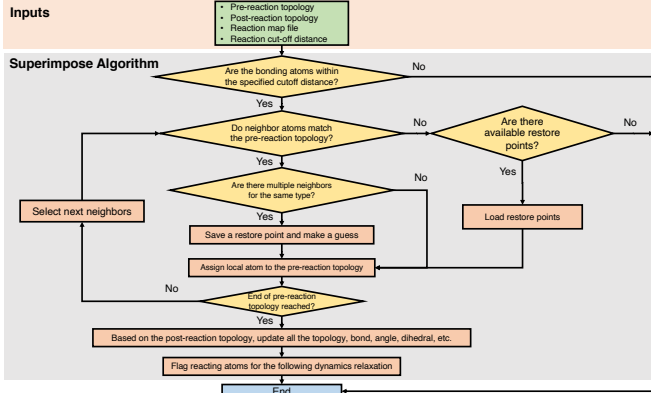


Figure 4. Summary of the crosslinking superimpose algorithm.

### B. Pull-out simulation

A series of pull-out test simulations were carried out using SMD, which efficiently quantifies the equilibrium properties (potential of mean force (PMF)) from a nonequilibrium process, in order to determine the IFSS between the nanofiber and the matrix. To assimilate the AFM pull-out test, an external force was applied in the SMD simulation an external force is applied to the end of the EPDM nanofiber in constant velocity mode by tethering a spring to one end of the EPDM nanofiber. A restoring force,  $F$ , was applied to the center of mass of the EPDM nanofiber atoms given by:

$$F = \nabla U = K[\nu t - (R(t) - R_0)] \left( \frac{m_i}{m} \right), \quad (3)$$

In the above,  $K$  is the spring constant,  $R_0$  is the initial equilibrium position of the center of mass (COM) of the loading region,  $R(t)$  is the position of the COM of the loading region at time  $t$ ,  $m_i$  is the mass of the atom,  $\nu$  is the pulling rate and  $m$  is the total mass of the nanofiber system.  $R(t)$  was incremented monotonously according to the pulling velocity. The work done during the SMD simulation was averaged over multiple independent configurations based on Jarzynski's nonequilibrium equality for free energy differences along the pulling path to compute the PMF [6]. The PMF was then considered as the pull-out energy,  $W_{\text{pull-out}}$ . The average IFSS can be estimated by:

$$\tau = \frac{W_{\text{pull out}}}{\int_0^L 2\pi r(L-x)dx} = \frac{W_{\text{pull out}}}{\pi r L^2} \quad (4)$$

where  $r$  and  $L$  are the radius and the embedded length of the nanofiber, respectively. The boundary conditions of the pull-out test are depicted in Fig. 5.

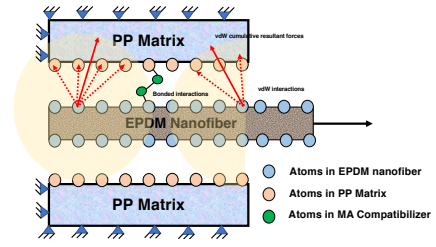


Figure 5. Boundary conditions of the pull-out test: the movement of the all sides of the matrix are fully constrained, while the left end of the nanofiber is free, and the right end is pulled-out

## IV. RESULTS AND DISCUSSION

### A. Nanostructure Evolution during coalescence

The nanostructural evolution of the nanofiber pair system can be analyzed by investigating the radial mass density. To measure the radial mass density, the nanofiber was divided into a finite number of cylindrical bins, as schematically depicted in Fig. 6a, and the corresponding radial mass densities were summed for all the atoms in the same bin. Fig. 6b illustrates the comparison between the normalized radial mass density profile of a single isolated nanofiber and a nanofiber from the nanofiber pair system. In the case of a single isolated nanofiber, the radial mass density increases as it approaches the core of the nanofiber. In contrast, the maximum radial mass density is extended outward from the core of the nanofiber pair system. Also, the cross-sectional contour plot of mass density for a nanofiber-pair system is illustrated in Figs. 6c-e. These results indicate that the polymeric chains tend to transfer from one nanofiber to the other, leading to the coalescence (see, Fig. 6e).

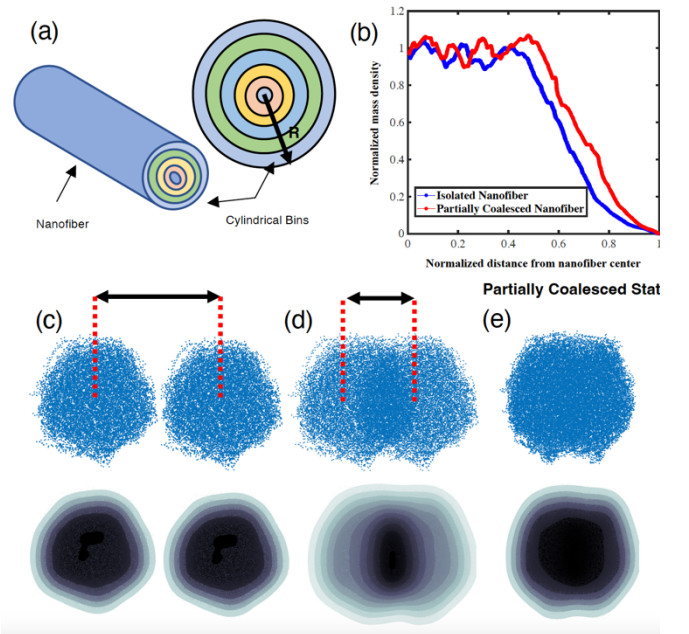


Figure 6. (a) nanofiber is divided into the finite number of cylindrical bins in order to calculate the radial mass density, (b) the normalized radial density of the single isolate nanofiber compared with the coalesced nanofiber, and (c-e) density contour plot at different simulation time.

## B. Interfiber Interaction Model

By comparing the total potential energies between systems with a nanofiber pair and a single isolated nanofiber, the interfiber interaction energy can be estimated. Fig. 7a shows the potential energy as a function of the separation distance normalized by the diameter of the nanofibers,  $s/2R$ . For a simulation time longer than about  $2\mu s$ , the potential energy varies exponentially between a maximum value, which is equal to the potential energy of the single isolated nanofiber ( $E_{\text{isolated}}$ ), and a minimum value equal to the potential energy of the coalesced nanofiber ( $E_{\text{pair}}$ ). A nanofiber pair system with a large separation distance can be considered as a single isolated nanofiber, and its linear density is half of the linear density of a coalesced nanofiber. To obtain the interfiber interaction energy,  $E_{\text{isolated}}$  was subtracted from the total potential energy,  $E_{\text{pair}}$ .

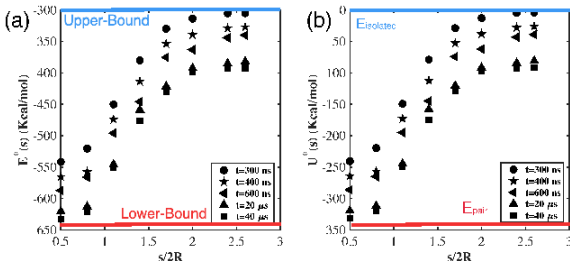


Figure 7. (a) Potential energy for the nanofiber-pair system as a function of the normalized separation distance,  $s/2R$  (the upper and lower lines are limits for the single isolated nanofibers and coalesced nanofibers), and (b) interfiber interaction energy as a function of the  $s/2R$ .

A mathematical function  $U(s^*)$ , describing the interfiber interaction energy as a function of their normalized separation distance was obtained from the curve fitting:

$$U(s^*) = U_0 + (U_\infty - U_0) \left[ \exp\left(-\frac{s^* - s_0^*}{\sigma}\right) \right]^{-1}, \quad (5)$$

In the above,  $s_0^*$  and  $\sigma$  are fitting parameters,  $s^*$  is the normalized separation distance ( $s/2R$ ), and  $U_0$  and  $U_\infty$  values are the lower and upper bounds of the interaction energies, as marked in Fig. 7b. Equation (5) predicts that within a certain separation distance, nanofibers are subjected to a force which drive them into the contact, with a work of adhesion of the order of  $U_\infty - U_0$ .

## C. Pull-out and Uniaxial Tension Simulations

In this section, two different EPDM/PP nanocomposite systems are considered, with and without surface modification with the MA compatibilizer grafting, to investigate the effect of the surface modification. To do this, the nanofiber was pulled-out of the PP matrix in the z-direction along the nanofiber axis (see, Figs. 8a-b). The IFSS was obtained using Eq. (5) and plotted with respect to the pull-out distance (Fig. 8c). The IFSS obtained for the systems with and without compatibilizer were calculated to be 32.16 MPa and 22.12 MPa, respectively. The lower IFSS for the system without compatibilizer is the result of the poor interfacial adhesion caused by the lack of chemical bonding at the interface. This will further hinder the local load transfer between the EPDM nanofiber and PP matrix. The load transfer is highly affected by stretching of interfacial polymeric chains that are chemically attached to the compatibilizer groups by means of mechanical unfolding, and subsequent detachment

from the EPDM nanofiber during the pull-out. Two sudden drops in the IFSS graph were also observed for the system with compatibilizer at small pull-out distance. These drops can be attributed to the deformation and stretching of the compatibilizer groups and release of their elastic energy (see, Fig. 8d), and also the energy dissipation associated with the plastic deformation of the EPDM polymer network. The fluctuation of the results, especially after the critical IFSS, is due to the surface roughness of the EPDM nanofiber and the presence of nanomechanical interlocking between the nanofiber and matrix. It has also been observed that, during the pull-out test, for the surface modified nanofiber, the strong chemical bonding, at the interface, transfers stress more efficiently from the matrix to the nanofiber and this leads to the nanofiber failure rather than interface debonding. During the pull-out test, the EPDM polymer system tries to minimize the effect of the applied load by changing the chain conformation via extension and reorientation mechanisms. However, when the interfacial adhesion is strong in the case of surface-modified crosslinked EPDM nanofiber, the conformation freedom is dramatically limited at the interface. So, although during the initial steps of loading, randomly oriented EPDM chains tend to re-orient themselves parallel to the pulling direction, their mobility is substantially limited and non-uniform. The reorientation reduces the entropy and increases the structural ordering. Since most of the chains are in coiled conformation, extra loading leads to the extension of EPDM polymeric chains. This extension of polymeric chains is highly dependent on the (i) interfacial strength and (ii) crosslinking density. Due to the presence of crosslinked chains and non-uniform strong adhesion at the interface, the extension of polymer chains is non-uniform and limited. This leads to the development of spatial heterogeneity, non-uniform density, and accumulation of stress in the system. As a result, nanovoids may start to develop near the interface, then they come into contact [7]. This may result in the formation of bigger voids which eventually causes full system failure during the last steps of loading.

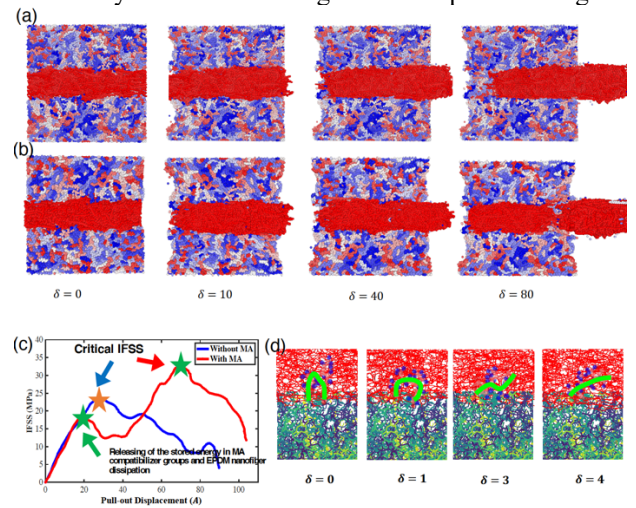


Figure 8. Simulation snapshots of the pull-out test with a constant speed that are taken at different pull-out distances: (a) without compatibilizer, (b) with compatibilizer, (c) IFSS vs. pull-out distance, and (d) deformation and stretching of the MA groups (green lines) corresponding to the released elastic energy at the early steps of the test.

Furthermore, longitudinal uniaxial tension simulation test for the systems with and without compatibilizer are depicted in Fig. 9. For both systems, the stress increases linearly with respect to strain until the tensile strength of 36.1 MPa and 32.8 MPa. A slight increase of tensile strength was observed for the system with compatibilizer. This is attributable to the enhanced local load transfer between nanofiber and matrix in the case of strong chemical bonding at the interface. After peak values of 36.1 MPa and 32.8 MPa for the two systems, the stress decreases and fluctuates due to unstable crack growth and initiation of the inter and intramolecular bond dissociation in the system [7]. To investigate the crack growth, the atomic concentration profiles of the nanocomposite systems at 41% strain were calculated by analyzing the deformation trajectories, and the corresponding results are plotted in Fig. 9b. In the atomic concentration profiles, the “lowest values” demonstrated by blue and red arrows in Fig. 9b for systems with and without compatibilizers, respectively, can be interpreted as the indicators for internally initiated breakages in the systems resulting from the non-bonded interactions dissociation which will further lead to localized topological failure. In the nanocomposite system without compatibilizer, due to the poor adhesion between nanofiber and matrix, interfacial debonding was observed near the middle and end of nanofiber, as failure initiations depicted by green circles in Fig. 9d.

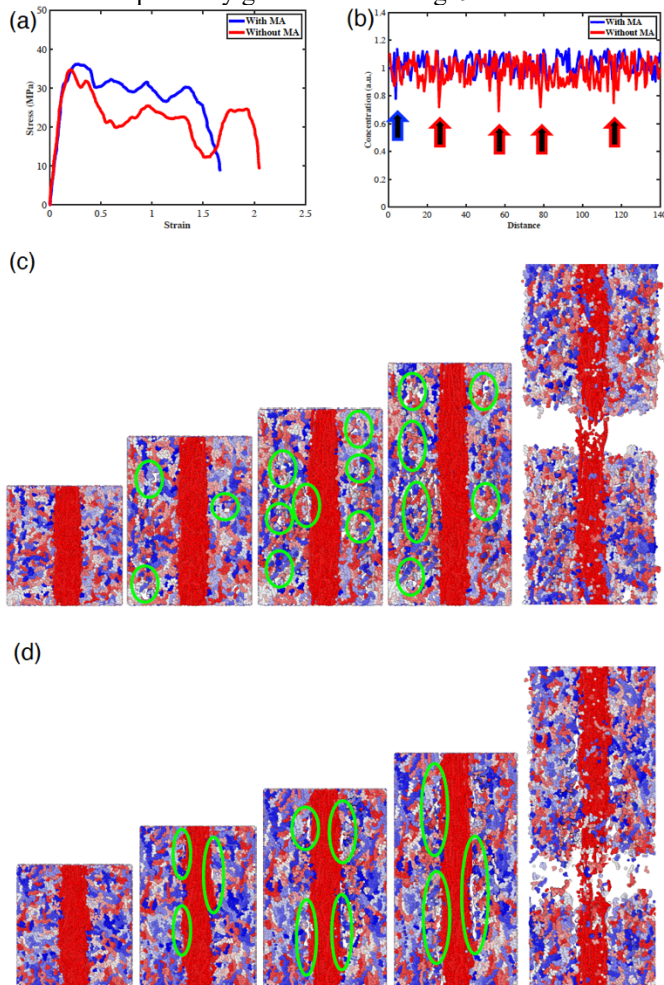


Figure 9. Longitudinal uniaxial tension simulation results: (a) stress-strain relations, and (b) concentration profiles. Failure mechanism for the system: (c) with compatibilizer, and (d) without compatibilizer.

## V. CONCLUSION

A theoretical and atomistic modeling scheme for the analysis of the effects of interface on the toughening and failure mechanisms of EPDM/PP nanocomposite systems is presented. This includes SMD simulations of EPDM/PP nanocomposite subjected to pull-out and uniaxial extension test. Emphasis was placed on the generation of a more comprehensive atomistic descriptions of nanocomposite systems, while maintaining efficiency and robustness in the corresponding numerical analyses. The interfiber interactions among polymeric nanofibers were also simulated to obtain the interaction potential between adjoined nanofibers, which may be further integrated into the continuum-based modeling and analysis of randomly oriented nanofiber reinforced polymer-based nanocomposites. The proposed atomistic model demonstrated that the presence of a small amount well-dispersed nanofibrillar network significantly affects the overall fracture toughness. The MD results also predicts that the IFSS can be enhanced by 30.9% with the MA compatibilizer grafting. The results are also closely aligned with experimental observations in PP nanocomposites toughened with rubber nanofibers in that, BDT of PP matrix can be achieved at low EPDM contents without deteriorating stiffness and yield strength. The atomistic simulation result predicts that MA compatibilizer restricts the motions of polymer chains at and in the vicinity of the nanofibers so that the formation of nanovoids and their coalescence in the nanocomposites are reduced.

## REFERENCES

- [1] M. Zeidi and C. IL Kim, “Mechanics of fiber composites with fibers resistant to extension and flexure,” *Math. Mech. Solids*, vol. 24, no. 1, pp. 3–17, Jan. 2019, doi: 10.1177/1081286517728543.
- [2] A. R. Alian, S. El-Borgi, and S. A. Meguid, “Multiscale modeling of the effect of waviness and agglomeration of CNTs on the elastic properties of nanocomposites,” *Comput. Mater. Sci.*, vol. 117, pp. 195–204, May 2016, doi: 10.1016/j.commatsci.2016.01.029.
- [3] M. Zeidi and C. Il Kim, “The Effects of Intra-membrane Viscosity on Lipid Membrane Morphology: Complete Analytical Solution,” *Sci. Rep.*, vol. 8, no. 1, p. 12845, Dec. 2018, doi: 10.1038/s41598-018-31251-6.
- [4] C. Zhao, L. H. Mark, M. Alshrah, I. Soltani, P. C. Lee, and C. B. Park, “Challenge in manufacturing nanofibril composites with low matrix viscosity: Effects of matrix viscosity and fibril content,” *Eur. Polym. J.*, vol. 121, p. 109310, Dec. 2019, doi: 10.1016/j.eurpolymj.2019.109310.
- [5] S. Buell, G. C. Rutledge, and K. J. V. Vliet, “Predicting polymer nanofiber interactions via molecular simulations,” *ACS Appl. Mater. Interfaces*, vol. 2, no. 4, pp. 1164–1172, 2010, doi: 10.1021/am1000135.J. Clerk Maxwell, *A Treatise on Electricity and Magnetism*, 3rd ed., vol. 2. Oxford: Clarendon, 1892, pp.68–73.
- [6] C. Jarzynski, “Nonequilibrium equality for free energy differences,” *Phys. Rev. Lett.*, vol. 78, no. 14, pp. 2690–2693, 1997, doi: 10.1103/PhysRevLett.78.2690.
- [7] M. Zeidi, C. Il Kim, and C. B. Park, “The role of interface on the toughening and failure mechanisms of thermoplastic nanocomposites reinforced with nanofibrillated rubber,” *Nanoscale*, vol. 13, pp. 20248–20280, 2021, doi: 10.1039/d1nr07363j.